Applications of least-squares pre-stack depth migration in complex geology around the world

Shouting Huang[1], Zhao Wang[1], Ming Wang[1], Adel Khalil[1], Ping Wang[1], Xiaodong Wu[1], Yi Xie[1], Francesco Perrone[1] and Chu-Ong Ting[1*] demonstrate the challenges that need to be overcome to achieve the ultimate goals in seismic imaging.

Introduction

Pre-stack depth migration has been an industrial imaging standard for decades, starting from the adoption of Kirchhoff migration in the early Nineties to the emergence of reverse-time migration (RTM) in the late 2000s. These algorithms map the recorded seismic reflection energy from a surface location to a subsurface location, through either a ray-based travel-time table or a wave-equation-based propagation engine. In principle, by combining high-fidelity migration algorithms and accurate subsurface velocity models, we can achieve the ultimate goals of seismic imaging: the correct positioning and focusing of the seismic reflectivity of the subsurface geological structures.

In reality, however, there are several challenges and issues that need to be addressed before we are able to achieve such an objective, not to mention the fact that most of the time we do not record all subsurface reflections sufficiently owing to limited coverage and sampling of the seismic recording spread. We can consider recorded seismic data to be the result of forward modelling experiments through subsurface structures. To image the reflectivity of the subsurface, we need to reverse the forward wave-propagation effects with an inverse of the forward modelling operator. Essentially, this is an inversion process. However, conventional imaging algorithms are formulated as adjoint operators rather than as true inverses (Claerbout, 1992). This approximation caused image degradation due to irregular and aliased acquisition sampling, limited receiver coverage, noise, and inhomogeneous or poor illumination caused by complex overburden. As a result, standard pre-stack depth migration algorithms suffer from migration artifacts with uncancelled swings, limited bandwidth, and distorted amplitude on subsurface reflectors (Gray, 1997). This is true even for state-of-the-art imaging technology such as RTM (Baysal et al., 1983; Zhang and Zhang, 2009).

Implementation and benefits of least-squares migration

Least-squares migration (LSM), which aims to recover the Earth's true reflectivity by obtaining the inverse of the forward modelling operator by minimizing the square of the misfit between the recorded data and the modelled data, was proposed to overcome the limitations of standard migration (Tarantola, 1987; Schuster, 1993; Nemeth et al., 1999). Conventional LSM is typically implemented as an iterative inversion procedure involving a looping of migrations and demigrations, which requires a significant number of iterations to converge, and is therefore computationally expensive. In practice, this approach is highly sensitive to noise in the data, velocity uncertainty, and other unexplained misfits.

To improve LSM's efficiency and robustness, various authors have proposed single-iteration LSM methods by estimating the inverse of the demigration-remigration operator (i.e., the so-called Hessian operator) using approaches such as point spread functions or non-stationary matching filters (Hu et al., 2001; Guitton, 2004; Lecomte, 2008; Valenciano et al., 2009; Fletcher et al., 2016). More recently, we (Wang et al., 2016) proposed using a 3D curvelet-domain matching filter to approximate the Hessian inverse. In addition to the usual benefits of LSM that compensate for illumination variations and acquisition footprint effects, curvelet formulation is also effective at attenuating random noise and migration swings by decomposing data into different frequency bands and dips. For only 2-3 times more cost than conventional migration, single-iteration LSM with curvelet-domain Hessian filtering (LSM-CHF) offers an affordable imaging algorithm in practice.

We first tested this approach on the SEG 3D SEAM I model. Figure 1 illustrates the procedure for single-iteration LSM on synthetic data. We started from a conventional RTM result on the left, which suffers from migration artifacts and uneven illumination. By performing a full demigration-remigration, we obtained the image with an extra imprint of illumination variations and migration artifacts. The inverse demigration-remigration operators can be directly derived by matching (b) to (a) in the 3D curvelet domain. Application of this filter on a conventional migration image produces the single-iteration LSM result on the right. We observe that LSM recovers the amplitude losses beneath the central salt body and yields an overall balanced reflectivity section. The impact of LSM is most prominent in the pre-stack domain.

To demonstrate this, we repeated the same process on RTM surface offset gathers (SOGs) (Yang et al., 2015), shown in Figure 2. The LSM gathers on the right show a reduction in the amplitude variations found on the conventional migration gathers on the left, which are caused by overburden focusing and

[1] CGG
* Corresponding author, E-mail: chu-ong.ting@cgg.com

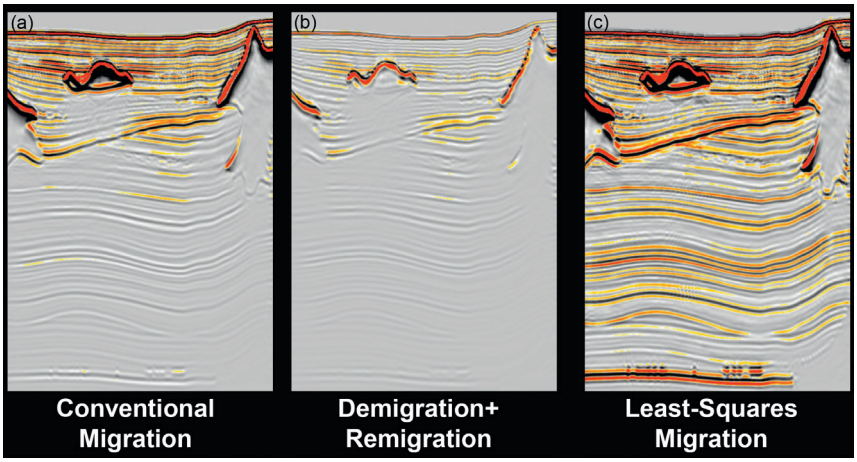

Figure 1 Synthetic illustration of single-iteration least-squares migration (LSM). We started from a conventional PSDM (a), and performed a full demigration-remigration to obtain image (b), which suffers from increased illumination variations and migration artifacts. The inverse Hessian operator was derived by matching (b) to (a) in the curvelet domain. Application of this filter on (a) led to the single-iteration LSM result (c).

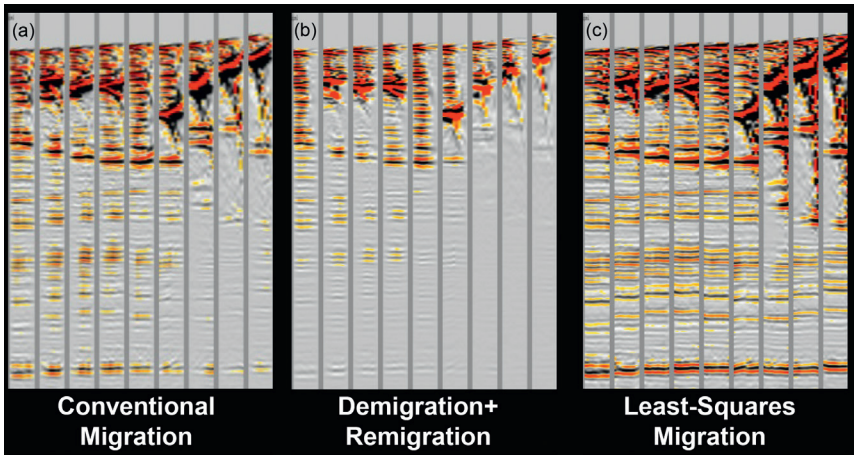

Figure 2 Application of single-iteration LSM on RTM surface offset gathers. An inverse Hessian operator is derived and applied for each individual offset in order to correct offset-dependent amplitude variations caused by shallow overburdens and acquisition footprint.

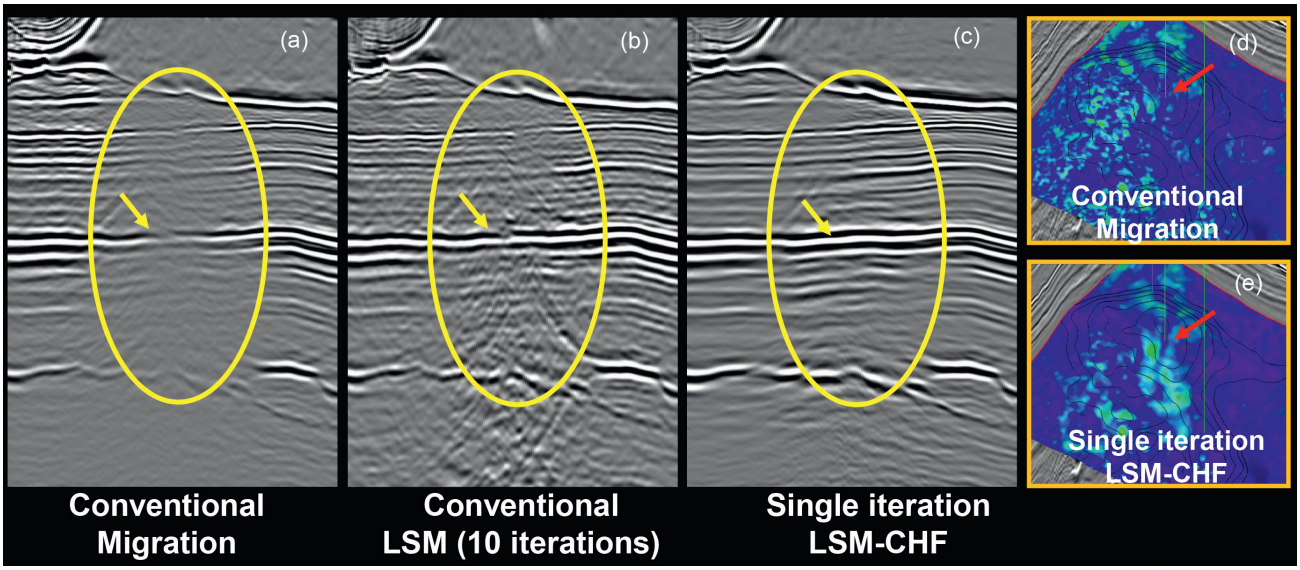

Figure 3 Application of LSM on a subsalt target located at a depth of 8-10 km. Here we compare (a) conventional migration, (b) conventional iterative LSM (with 10 iterations), and (c) our proposed LSM-CHF. While both least-squares migrations improve the amplitude balance, conventional iterative LSM poorly handles the noise. On the contrary, LSM-CHF improves the signal-to-noise ratio by compensating for amplitude losses on the signal component only. We extracted the amplitude at a target event for (d) conventional migration and (e) single-iteration LSM-CHF. The red arrows point to potential channels across the reservoir, whose positions were uncertain on the conventional migration image.

de-focusing effects, as well as a general offset-dependent amplitude bias introduced by acquisition sampling. Generally, the gathers become more suitable for picking and subsequent tomographic velocity updating or amplitude-versus-offset (AVO) analysis. We note, however, that this test is not realistic because we did not include noise in the synthetic data, and we have used the exact velocity model. The reality and possibilities for LSM would be better examined using field data in a more realistic

context, i.e., with an inevitably inaccurate velocity model and in the presence of noise, especially in a complex geology setting.

Application on subsalt imaging and 4D processing

It is well known that complex salt bodies in the Gulf of Mexico (GoM) cause strong illumination distortion on target subsalt reservoirs, which affects the reliability of quantitative amplitude analysis. Here, we applied LSM on a deepwater wide-azimuth streamer data set from Keathley Canyon, GoM. The input data underwent typical preprocessing to remove noise, ghost energy, multiples, etc. The Eocene-Cretaceous reservoir sits at a depth of 9-10 km and lies beneath a 4-5 km-thick salt body. Figure 3a shows that even with wide-azimuth data, the subsalt image with conventional migration still suffers from uneven illumination with visible migration artifacts. The yellow circle outlines a problematic area with lower signal-to-noise ratio and amplitude dimming artifacts caused by the complex overburden. In this data set, we tested both conventional iterative LSM (Figure 3b) and our proposed single-iteration LSM-CHF (Figure 3c). While both methods were effective at reducing subsalt amplitude distortion, single-iteration LSM-CHF performed better in terms of handling noise than conventional iterative LSM. In this example, the conventional iterative LSM was performed with up to ten iterations, which is approximately ten times more costly than single-iteration LSM. To investigate the impact on interpretation, we extracted the amplitude at a target structure within the yellow circle for both conventional migration and single-iteration LSM-CHF. The red arrows in Figures 3d and 3e show how the channel system becomes more interpretable with the amplitude extracted from the single-iteration LSM-CHF.

Because of its ability to mitigate acquisition-related effects, LSM is naturally suited for 4D imaging. To adapt LSM to a conventional 4D processing sequence, we (Wang et al., 2017) proposed the workflow illustrated in Figure 4. The workflow estimates the inverse Hessian filters separately for the baseline and monitor surveys using a common reflectivity model, which can be an optimized stacked volume of baseline and monitor migration volumes, since it has the best signal to stabilize the inverse filter estimation. The demigration-remigration process is performed with the same velocity model for each individual survey geometry to ensure any 4D-related time shifts are kept after LSM for analysis by interpreters using a conventional 4D analysis workflow. Once we apply LSM on each survey, the 4D difference can be obtained by subtracting the individual 3D LSM images.

Alternatively, this method can be extended to joint multi-vintage LSM, which incorporates 4D reflectivity changes as part of the least-squares inversion process. However, this needs further modification to accommodate any 4D velocity changes between the surveys, so it goes beyond the scope of least-squares migration. The advantages of our current workflow are threefold: firstly, it does not affect well established 4D pre-processing or inversion sequences, so risk is minimal. Secondly, we will, by default, have a better 3D volume from single-iteration LSM for any 3D interpretation work. Thirdly, the LSM result is naturally cleaner so it potentially saves considerable effort on post-migration data conditioning.

We demonstrated the effectiveness of the 4D LSM workflow on a challenging ocean bottom seismic (OBS) to narrow-azimuth towed-streamer (NATS) 4D processing project for the Conger field in the GoM (Wang et al., 2017). The prospect is a subsalt Upper Miocene reservoir with rich gas condensates. The existing seismic data over this area include a pre-production narrow-azimuth streamer survey acquired in 1995 and a full-azimuth OBS survey acquired in 2013. Despite very poor repeatability between the two surveys, clear and credible 4D signal was observed after intense processing efforts (Wei et al., 2016; Stieglitz et al., 2016).

To apply LSM on the 4D imaging, we followed the above-mentioned workflow. Both data sets were 4D co-processed to final Kirchhoff migration. We then built a common reflectivity model by combining the migration results from the NATS and OBS surveys. Using the common reflectivity model, Kirchhoff demigration and remigration were performed for the NATS and OBS data separately. The inverse Hessian filters were estimated individually for NATS and OBS by matching their respective demigration-remigration results to the common reflectivity model. Once we had obtained both OBS LSM and NATS LSM volumes, we calculated the 4D LSM difference by simply subtracting the two volumes.

Figure 5 shows a comparison of 4D differences generated from conventional OBS-NATS Kirchhoff volumes and least-squares OBS-NATS Kirchhoff volumes. LSM improves the 4D image in two ways: firstly, it reduces 4D noise by compensating for acquisition geometry differences between baseline and monitor and by reducing non-repeatable ambient noise. Secondly, LSM improves the 4D signal by reducing reservoir amplitude distortions owing to complex overburden such as salt or shallow gas zones. The 4D RMS signal is more coherent with LSM, as shown in Figure 5d. Potentially, this could have a bigger impact on those fields with a weak expected 4D signal.

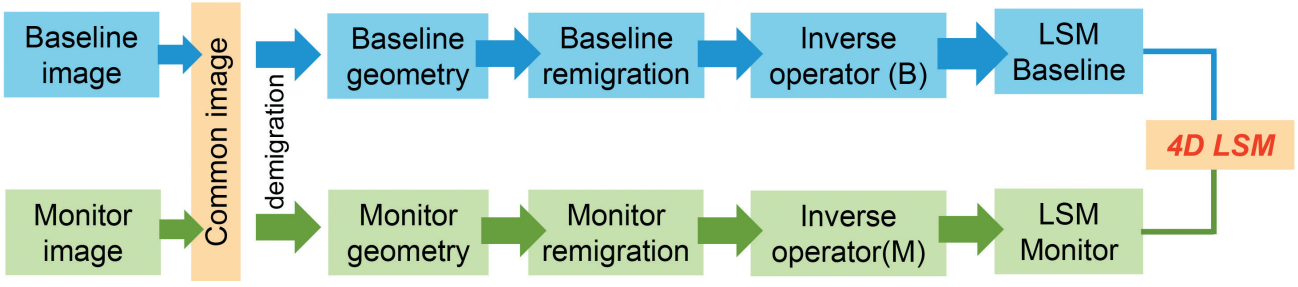

Figure 4 LSM for a 4D imaging workflow. We derived inverse operators independently by demigrating a common image onto each acquisition geometry. These operators not only correct acquisition geometry-related effects on both baseline and monitor images independently, but also correct illumination distortion associated with each acquisition layout. Once we apply LSM on each survey, the 4D LSM difference can then be obtained by subtracting individual 3D LSM images.

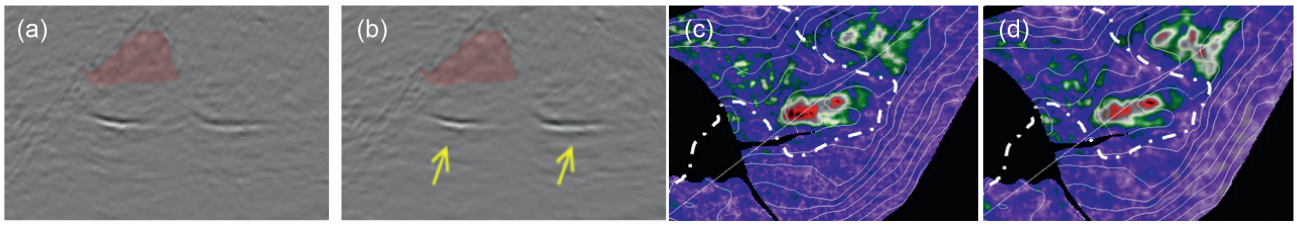

Figure 5 OBS-NATS 4D difference: (a) 4D stack differences between standard Kirchhoff volumes and (b) LSM Kirchhoff volumes. The red shaded area indicates a salt body, and the yellow arrows point to 4D signals. 4D RMS signal at the Conger target reservoir horizon from (c) standard Kirchhoff and (d) LSM Kirchhoff. The white dashed line outlines the salt edge, which indicates part of the reservoir covered by salt.

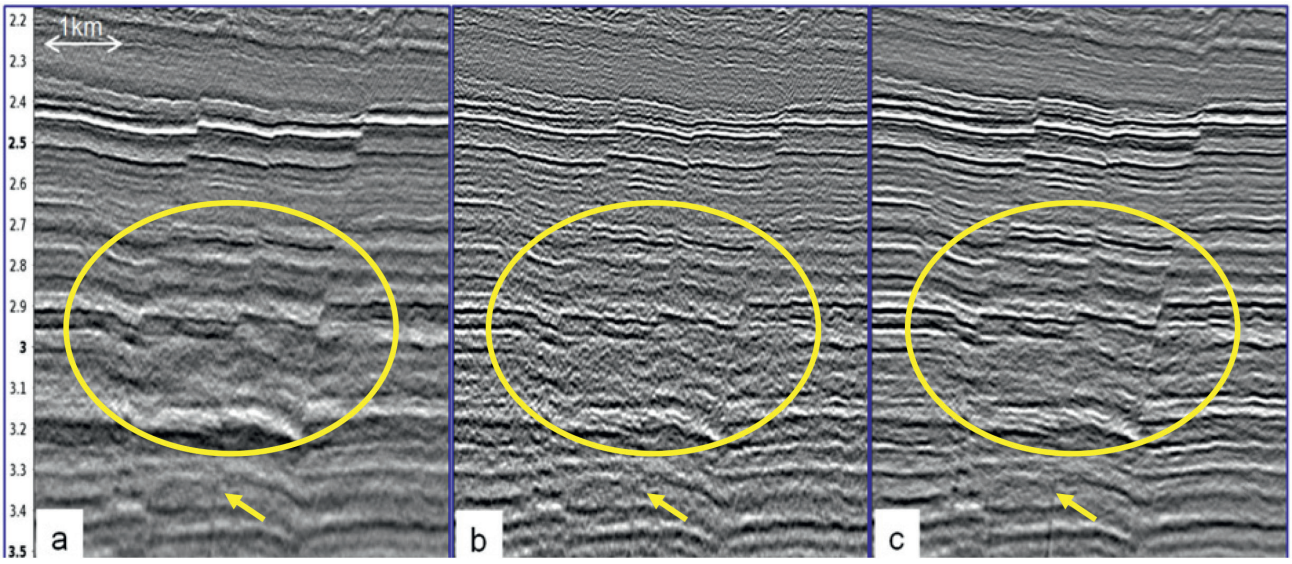

Figure 6 Comparison of common-offset migrated sections: (a) Conventional migration, (b) QPSDM, (c) LS-QPSDM.

Correcting absorption effects with least-squares Q migration

Besides adapting LSM to different types of acquisition geometry, we also expand the physics to accommodate absorption effects caused by the anelastic nature of the Earth, which affects the amplitude, frequency, and phase accuracy of the recorded reflectivity. Conventional Q pre-stack depth migration (QPSDM) has been an industry workhorse, compensating for absorption losses by accurately estimating the amplitude and phase distortion along raypaths. However, the frequency-dependent correction often overboosts noise and migration artifacts, thus masking steeply dipping faults and weak reflectors. Conversely, single-iteration LS-QPSDM is able to correct both absorption and illumination distortion while mitigating noise levels (Wu et al., 2017; Shao et al., 2017; Casasanta et al., 2017).

The extension of LSM in this case is straightforward by incorporating the absorption effect in both the migration and demigration processes, and both the theory and implementation have been discussed extensively by Casasanta et al. (2017).

We applied the proposed LS-QPSDM approach to a marine narrow-azimuth field data set from NWS Australia. For this data set, a background earth absorption Q of 150 had been estimated. Single-offset results from various migrations (~2 km offset) are shown in Figure 6. Figure 6a is the conventional migration section without considering Q. This image lacks high frequencies, and resolution is lost due to the Earth's absorption. QPSDM and LS-QPSDM are presented in Figures 6b and 6c. Both methods are able to compensate for high-frequency loss and improve resolution, but QPSDM suffers from migration artifacts and the faults are masked by overboosted noise (yellow arrows). In contrast, LS-QPSDM provides sharper faults and the migration artifacts within the circled area are reduced. It yields an overall improved image over conventional migration.

To test it on different geology, we performed LS-QPSDM on a 3D variable-depth marine streamer data set acquired in Quad 22 of the UKCS Central North Sea. The data set underwent a broadband pre-processing sequence (Hollingworth et al., 2015) and achieved good-quality low-frequency data due to a deeper tow depth down to 50 m. In Figure 7a, we show a near-offset (~500 m) Kirchhoff depth-migrated section containing a salt diapir rising through the upper Cretaceous chalk, with residual migration swing energy indicated by the yellow arrow. The resolution inside the chalk section is limited, as indicated by the blue arrow. Comparing conventional migration with LS-QPSDM (Figures 7a and 7b), we see a degree of uplift in event continuity, improved resolution, and reduced noise and swing artifacts. LS-QPSDM also offers more balanced illumination and a stable increase in resolution.

To further analyse the benefits of LS-QPSDM, we investigated reservoir attributes by performing a pre-stack inversion on this broadband data set. Figure 8 shows an acoustic impedance (Ip) and Vp/Vs ratio comparison between the inversion results of conventional Kirchhoff migration and LS-QPSDM. The vertical time axis ranges between 2.5 and 4 s, and the colour map was chosen to highlight areas of interest below the Base Cretaceous Unconformity (BCU). The white circles indicate an area with improved

resolution and coherency in the LS-QPSDM. The definition of the low Vp/Vs zone is clearer and sharper in the LS-QPSDM than the conventional Kirchhoff. In general, low-frequency vertical striping noise is reduced in the LS-QPSDM, yielding a section with greater lateral continuity in these attributes, as indicated by the white arrows. Coherency of acoustic impedance (Ip) demonstrates the benefit on the stack image, while the Vp/Vs coherency indicates the consistency across offsets.

Conclusions

We have shown that single-iteration LSM with curvelet-domain implementation is able to deliver the promises of least-squares migration on various real data sets. The direct application of LSM on subsalt prospects leads to images with more balanced illumination, improved signal-to-noise ratio, and more interpretable seismic amplitudes. We have also demonstrated the benefits of LSM on challenging 4D projects, especially for highly non-repeatable vintages or prospects with weak 4D signal. To overcome amplitude distortion caused by absorption, we extended the approach to LS-QPSDM. The result is more reliable than conventional Q-PSDM owing to its natural mitigation of noise and the extra illumination correction.

Finally, the estimation of inverse Hessian operators through curvelet-domain matching can also be applied in the data domain (Khalil et al., 2016) and can be incorporated in the iterative LSM formulation (Wang et al., 2017). In the latter case, it was used as a preconditioner to significantly speed up the convergence rate of iterative LSM. As LSM comes over time to be validated on more synthetic and field data by our least-squares imaging community, we look forward to seeing new ideas and implementations that will eventually bring LSM to its full potential.

Acknowledgements

We would like to thank CGG's worldwide subsurface imaging production and R&D teams for their dedicated support and feedback, especially GPU code optimization from Yu Wang and

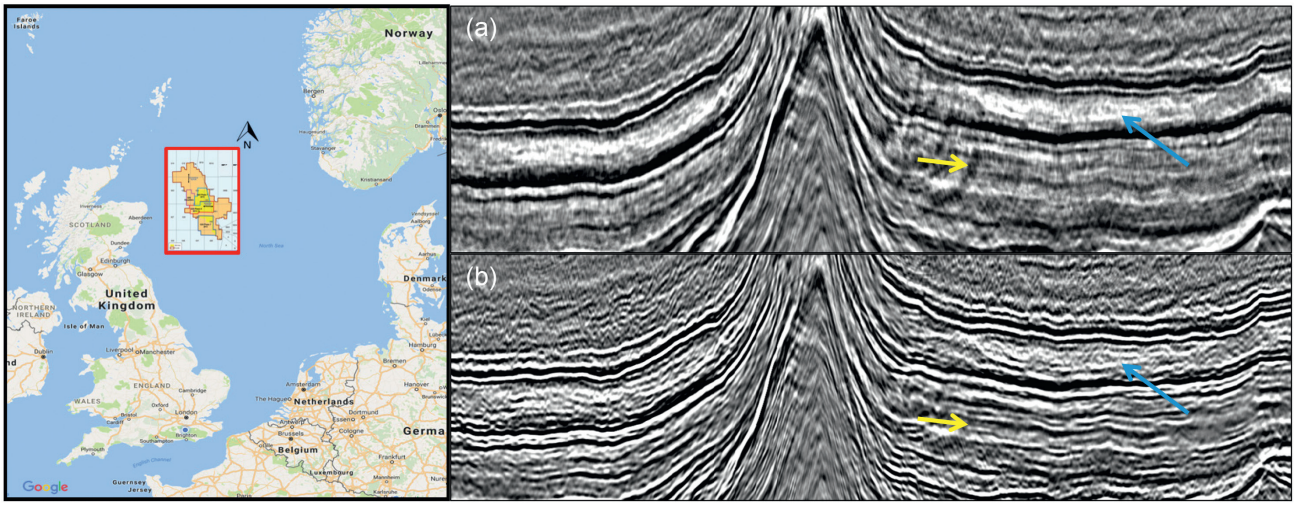

Figure 7 Comparison of common-offset migrated sections: (a) Conventional migration and (b) LS-QPSDM.

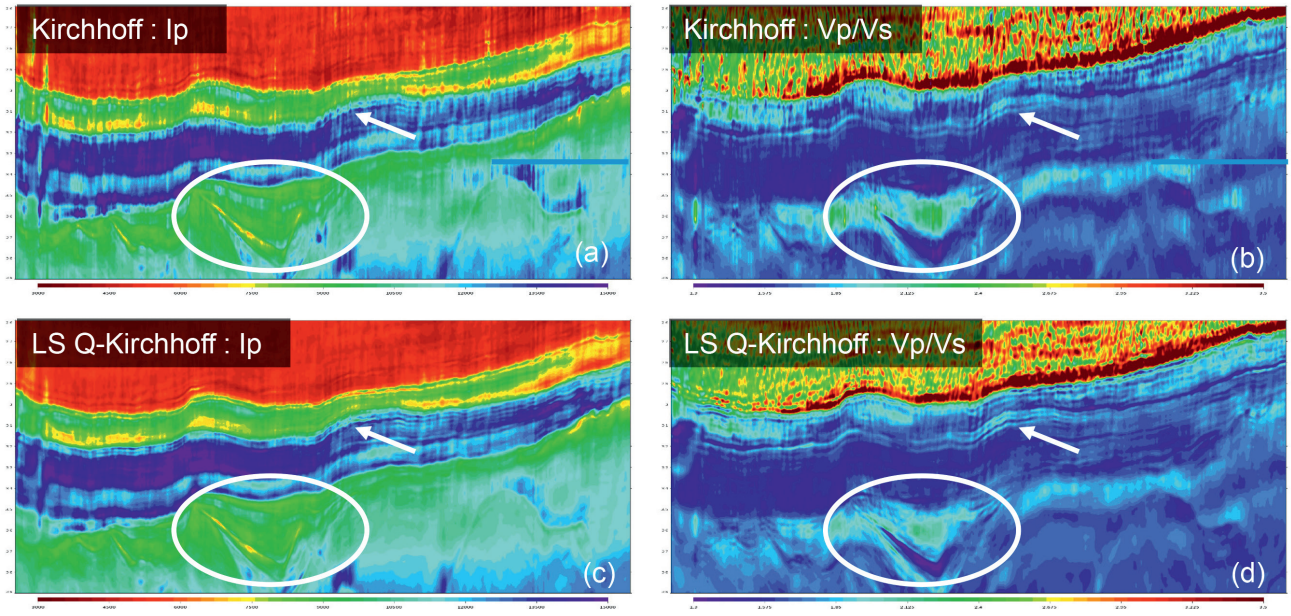

Figure 8 Comparison of acoustic impedance (Ip) and Vp/Vs of pre-stack inversion results from (a) conventional migration and (b) LS-QPSDM.

pre-stack inversion QC from Arash Jafargandomi. We would also like to thank CGG Multi-Client & New Ventures, Chevron, Shell, Anadarko, and Hess for giving us show rights permissions. We appreciate various discussions we have had with Lorenzo Casasanta, Andrew Ratcliffe, Graham Roberts, Adriano Gomes, and Zhigang Zhang. We also thank Yu Zhang, James Sun, and Richard Leggott for their early work on least-squares imaging within CGG.

References

Baysal, E., Kosloff, D. and Sherwood, J. [1983]. Reverse-time migration. *Geophysics*, **48** (11), 1514–1524, http://dx.doi.org/10.1190/1.1441434.

Casasanta, L., Perrone F., Roberts, G., Ratcliffe, A., Purcell, K., Jafargandomi A. and Poole, G. [2017]. Applications of single-iteration Kirchhoff least-squares migration. *SEG Technical Program Expanded Abstracts*, 4432-4437.

Claerbout, J.F. [1992]. *Earth soundings analysis: Processing versus inversion*. Blackwell Scientific Publications.

Fletcher, R.P., Nichols, D., Bloor, R. and Coates, R.T. [2016]. Least-squares migration – Data domain versus image domain using point spread functions. *The Leading Edge*, **35** (2), 157-162.

Gray, S.H. [1997]. True-amplitude seismic migration: A comparison of three approaches. *Geophysics*, **62** (3), 929–936.

Guitton, A. [2004]. Amplitude and kinematic corrections of migrated images for nonunitary imaging operators. *Geophysics*, **69** (4), 1017–1024, http://dx.doi.org/10.1190/1.1778244.

Hollingworth, S., Pape, O., Purcell, C., Kaszycka, E., Baker, T., Cowley, J., Duval, G. and Twigger, L. [2015]. Setting new standards for regional understanding – mega-scale broadband PSDM in the North Sea. *First Break*, **33** (9), 75-79.

Hu, J., Schuster, G.T. and Valasek, P.A. [2001]. Poststack migration deconvolution. *Geophysics*, **66** (3), 939–952, http://dx.doi.org/10.1190/1.1444984.

Khalil, A., Hoeber, H., Roberts, G. and Perrone, F. [2016]. An alternative to least-squares imaging using data-domain matching filters. *SEG Technical Program Expanded Abstracts*, 4188-4192, http://dx.doi.org/10.1190/segam2016-13861302.1.

Lecomte, I. [2008]. Resolution and illumination analyses in PSDM: A ray-based approach. *The Leading Edge*, **27** (5), 650–663, http://dx.doi.org/10.1190/1.2919584.

Nemeth, T., Wu, C. and Schuster, G.T. [1999]. Least-squares migration of incomplete reflection data. *Geophysics*, **64** (1), 208–221, http://dx.doi.org/10.1190/1.1444517.

Schuster, G.T. [1993]. Least-squares crosswell migration. *SEG Technical Program Expanded Abstracts*, 110–113, http://dx.doi.org/10.1190/segam2012-1425.1.

Shao, G., Zhuang, D., Huang, R., Wang, P., Nolte, B., Paramo, P. and Vincent, K. [2017]. Least-squares Q migration: the path to improved seismic resolution and amplitude fidelity. *SEG Technical Program Expanded Abstracts*, 4400-4404.

Stieglitz, T., Shi, C., Morton, S., Walker, D., Martins, W., Pujiyono, P. and Kuntz, B. [2016]. Illumination, Imaging and 4D Analysis of the Conger Field (GB 215). *SEG Technical Program Expanded Abstracts*, 3935-3939.

Tarantola, A. [1987]. *Inverse problem theory: Methods for data fitting and model parameter estimation*. Elsevier Science Publishing Company.

Valenciano, A.A., Biondi, B.L. and Clapp, R.G. [2009]. Imaging by target-oriented wave-equation inversion. *Geophysics*, **74** (6), WCA109–WCA120.

Wang, M., Huang, S. and Wang, P. [2017]. Improved iterative least-squares migration using curvelet-domain Hessian filters. *SEG Technical Program Expanded Abstracts*, 4555-4560.

Wang, P., Gomes, A., Zhang, Z. and Wang, M. [2016]. Least-squares RTM: Reality and possibilities for subsalt imaging. *SEG Technical Program Expanded Abstracts*, 4204-4209.

Wang, Z., Huang, R., Xuan, Y., Xu, Q., Morton, S. and Kuntz, B. [2017]. Improving OBS-streamer 4D imaging by least-squares migration. *SEG Technical Program Expanded Abstracts*, 5819-5823.

Wei, Z., Xuan, Y., Huang, R., Theriot, C., Rodenberger, D., Chang, M., Morton, S. and Zouari, M. [2016]. Application of deghosting for spectral matching in OBS-streamer 4D processing. *SEG Technical Program Expanded Abstracts*, 5506-5510.

Wu, X.D., Wang, Y., Xie, Y., Zhou, J., Lin, D., and Casasanta, L. [2017]. Least square Q-Kirchhoff migration: Implementation and application. *79th EAGE Conference & Exhibition,* Extended Abstracts, Tu A1 08.

Yang, Z., Huang, S. and Yan, R. [2015] Improved subsalt tomography using RTM surface offset gathers. *SEG Technical Program Expanded Abstracts*, 5254-5258.

Zhang, Y. and Zhang, H. [2009]. A stable TTI reverse time migration and its implementation. *SEG Technical Program Expanded Abstracts*, 2794-2798, http://dx.doi.org/10.1190/1.3255429.